ISSN 1560-3547, Regular and Chaotic Dynamics, 2024, Vol. 29, No. 1, pp. 120–133. © Pleiades Publishing, Ltd., 2024.
ISSN 1560-3547, Regular and Chaotic Dynamics, 2023. © Pleiades Publishing, Ltd., 2023.

Chaos and Hyperchaos in Two Coupled Identical Hindmarsh – Rose Systems

Nataliya V. Stankevich[1*], Andrey A. Bobrovskii[1], and Natalya A. Shchegoleva[1***]**

[1] *HSE University,*
ul. Bolshaya Pecherskaya 25/12, 603155 Nizhny Novgorod, Russia

Received April 28, 2023; revised September 12, 2023; accepted October 10, 2023

Abstract—The dynamics of two coupled neuron models, the Hindmarsh – Rose systems, are studied. Their interaction is simulated via a chemical coupling that is implemented with a sigmoid function. It is shown that the model may exhibit complex behavior: quasi-periodic, chaotic and hyperchaotic oscillations. A phenomenological scenario for the formation of hyperchaos associated with the appearance of a discrete Shilnikov attractor is described. It is shown that the formation of these attractors leads to the appearance of in-phase bursting oscillations.

MSC2010 numbers: 65P20, 92B25

DOI: 10.1134/S1560354723540031

Keywords: neuron model, Hindmarsh – Rose system, chaos, hyperchaos, in-phase bursting

1. INTRODUCTION

Ensembles of oscillators are one of the most important objects of study in nonlinear dynamics. The results of their investigation can find practical application in neurophysiology, cell biology, quantum physics, information and telecommunication systems, and other interdisciplinary sciences [1–7]. Their dynamics are rich and varied, due to a large number of nonlinear phenomena that arise as a result of the interaction. One of the most significant nonlinear effects is the synchronization phenomenon [5–7]. The theory of synchronization has been developing for many years, and new aspects of classical problems appear, often in the simplest basic models, the solution of which significantly enriches the fundamental ideas about the nonlinear dynamics of self-oscillating systems.

As a result of the interaction, the dynamics of the system can become more complex. For example, hyperchaos [8] can arise in a system of coupled chaotic oscillators. Such a phenomenon was found in the ring of Chua's circuits [9], in two Rössler systems coupled by linear diffusion of one variable [10–12], in Colpitts oscillators coupled by means of two linear resistors [13], and in coupled antiphase driven Toda oscillators [14].

For some special conditions it is also possible to obtain the occurrence of hyperchaos for interacting autooscillatory models with periodic regime. For instance, in the ring of unidirectionally coupled identical Duffing oscillators which are in stable steady state without coupling, hyperchaos can arise due to the presence of linear cross-diffusion coupling [15]. Another example is the ensemble of three genetic repressilators interacting via a quorum-sensing mechanism [16]. In this model oscillators are identical and strongly dissipative, but nonlinear coupling leads to a complexification of the dynamics and even to the appearance of hyperchaos. Moreover, this type of complex behavior

*E-mail: stankevichnv@mail.ru
**E-mail: piqzo1999@mail.ru
***E-mail: migunovanatasha@mail.ru

dominates for the model in parameter space. One more example is provided by the multi-circuit generator, which represents the ensemble of van der Pol oscillators coupled via a mean field [17]. For such kind of interaction it is possible to observe multi-frequency quasi-periodic oscillations and its destruction leading to hyperchaos.

In the present work, we consider the simplest ensemble of identical neuron models (two coupled oscillators) that demonstrate periodic oscillations in the autonomous case. The coupling of subsystems is organized through the sigmoid function, which has the physiological meaning of the chemical interaction of neurons via a synapse. Ensembles of neurons are of great interest to researchers due to their significance in applications [18–27]. In [28–32], it was shown that, given various types of interaction between subsystems (excitatory, inhibitory chemical and electrical), in-phase synchronization may occur. It is also shown that multistability between in-phase and antiphase oscillations is possible in such a system. In the present work, we study several features of irregular behavior resulting from the interaction. Computing the spectrum of Lyapunov exponents, we classify various types of chaotic dynamics, localize areas of chaos and hyperchaos, study scenarios for the emergence of hyperchaos and consider the characteristic features of the interaction of models demonstrating various periodic oscillations. We have shown that the appearance of in-phase synchronization of bursting oscillations is associated with hyperchaos formation via the absorption of a synchronous manifold represented by a saddle cycle with a two-dimensional unstable manifold.

The paper is structured as follows. In Section 2 we describe the object under consideration, present both autonomous and coupled models, their main parameters, and some dynamical regimes in the autonomous model. In Section 3 we demonstrate results of numerical simulation of two coupled neuron models, describe the scenario of hyperchaos occurrence, and explain how it is reflected on time series of the system. In Section 4 we depict the structure of the parameter plane of two coupled models for another value of parameters and discuss the universality of the results obtained.

2. OBJECT OF INVESTIGATION: INTERACTING NEURON MODELS WITH TWO TYPES OF CHEMICAL COUPLINGS

2.1. Autonomous System, Choice of Parameters

The Hindmarsh – Rose system is one of the well-known models that describe the dynamics of a neuron and reproduce a characteristic for neurons dynamical regimes [36–38] which can be written in the following form:

$$\begin{aligned} \dot{x} &= ax^2 - x^3 - y - z, \\ \dot{y} &= (a+\alpha)x^2 - y, \\ \dot{z} &= \mu(bx + c - z), \end{aligned} \tag{2.1}$$

where x is the membrane potential, the variables y and z characterize the transport of ions through the membrane through "fast" and "slow" ion channels, respectively, and a, b, c, α, μ are the model's parameters. The Hindmarsh – Rose system (2.1) exhibits a variety of oscillatory activity typical for neuron models: silent state, spiking and bursting oscillations. Bursting oscillations are the most interesting due to their significance for the functioning of neuron-like cells [33] and long-term benefits of neural coding with bursts [34].

According to [22], different types of bursting attractors are possible: square-wave bursting and plateau bursting attractors. Such kind of bursting attractors can also be observed in the Hindmarsh – Rose model. Figure 1 shows examples of two types of bursting attractors for various parameter values. The first column shows the three-dimensional phase portrait of the attractor, and the second column shows the time series for the variable x. We fixed the parameter as in [31]: $\alpha = 1.6$, $b = 9.0$, $c = 5.0$, $\mu = 0.001$; in this case, at $a = 2.8$, a periodic bursting attractor of square-wave type is observed. Figure 1a clearly shows that one burst contains 9 spikes. These parameters were studied in [31], where the authors showed the synergistic effect of the occurrence of in-phase

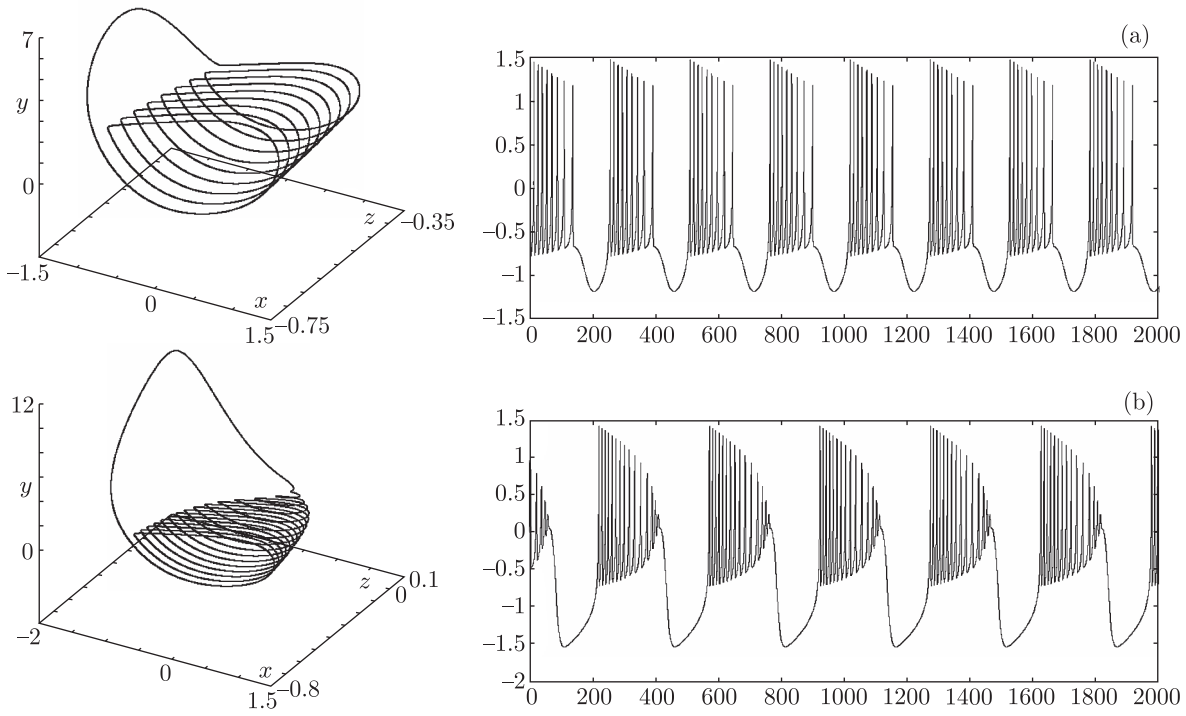

Fig. 1. Attractors in 3D phase space and time series demonstrating the characteristic dynamical regimes of the Hindmarsh – Rose model (2.1). Parameters: $\alpha = 1.6$, $b = 9.0$, $c = 5.0$, $\mu = 0.001$. (a) square-wave bursting attractor, $a = 2.8$; (b) plateau bursting attractor $a = 2.7$.

bursting oscillations when two types of chemical coupling were taken into account. By slightly reducing the parameter a, the type of the bursting attractor is changed. Figure 1b shows an example of a plateau bursting attractor with $a = 2.7$. The attractor here is still bursting; however, we see that the amplitude of oscillation in the bursts decreases. This change corresponds to the Andronov – Hopf bifurcation in the "fast subsystem" which can be obtained by assuming the slow variable to be constant. In the present work, we carry out a detailed analysis of interacting systems for the first case, when a square-wave bursting attractor is observed in system (2.1). Also, we present some illustrations for the second type of bursting attractor to demonstrate the versatility of the above-mentioned scenarios and the picture of dynamical regimes.

2.2. Model of Two Coupled Hindmarsh – Rose Systems

The interaction of neurons is carried out in various ways. Two types of couplings are well known: chemical and electrical. The chemical coupling is fast, and is implemented via a ligand. Electrical connection is slow and requires direct cell contact (the so-called gap-junction) [35]. In [31, 32] it is shown that the interaction through two types of chemical couplings, both excitatory and inhibitory, leads to the appearance of in-phase bursting oscillations, which is atypical for such systems. Typical synchronization is antiphase in accordance with the "winner-takes-all" principle [22]. Let us consider in more detail the mechanisms of formation of various attractors and types of synchronization.

The model of the Hindmarsh – Rose systems interacting via two types of chemical coupling can be written as follows:

$$\begin{aligned} \dot{x}_i &= ax_i^2 - x_i^3 - y_i - z_i + F(x_i, x_j), \\ \dot{y}_i &= (a + \alpha)x_i^2 - y_i, \\ \dot{z}_i &= \mu(bx_i + c - z_i), \end{aligned} \tag{2.2}$$

where $i, j = 1, 2$ are the numbers of interacting elements. The coupling function $F(x_i, x_j)$ contains two terms corresponding to two types of interactions:

$$F(x_i, x_j) = g_{exc}(V_{exc} - x_i)\Gamma(x_j) + g_{inh}(V_{inh} - x_i)\Gamma(x_j). \tag{2.3}$$

Fast synaptic (chemical) coupling can be simulated by the sigmoid function:

$$\Gamma(x_j) = \frac{1}{1 + e^{-\lambda(x_j - \Theta_S)}}. \tag{2.4}$$

Here Θ_S is the synaptic threshold, $\Theta_S = -0.25$. V_{exc}, V_{inh} are thresholds of excitatory and inhibitory couplings; for $V_{exc} = 2 > x_i(t)$ and $V_{inh} = -2 < x_i(t)$ excitatory or inhibitory coupling occurs for any $x_i(t)$, respectively. Thus, we have two parameters, using which we can control excitatory and inhibitory interaction between neurons. We have fixed the other parameters in the following way:

$$a = 2.8, b = 9.0, c = 5.0, \alpha = 1.6, \lambda = 10, \mu = 0.001. \tag{2.5}$$

In [39, 40] one can find results obtained for chemically coupled Hindmarsh – Rose models. Another interesting result for different types of couplings and topologies of the ensemble is presented in [39, 40].

3. INTERACTION OF NEURON MODELS WITH THE SQUARE-WAVE BURSTING ATTRACTOR

As mentioned above, the main goal of this work is to analyze the complex behavior of system (2.2), including chaotic and hyperchaotic ones. In this regard, the main tool for studying system (2.2) will be the analysis of the spectrum of Lyapunov exponents and the chart of Lyapunov exponents. These charts are constructed as follows. The parameter plane is scanned with some step. For each point of the parameter plane, after reaching the attractor, the full spectrum of Lyapunov exponents is calculated, and the point on the plane is assigned a color corresponding to their values. The Lyapunov exponents were calculated using the algorithm presented in [41] and the Gram-Schmidt orthogonalization. Table 1 shows the correspondence between the dynamical regime, the signature of the Lyapunov exponent spectrum and the colors, which will be further used in the Lyapunov exponent charts.

Table 1. Correspondence between the dynamical regimes, the signature of the spectrum of Lyapunov exponents, and the color in the charts

Dynamical regime	Signature of the Lyapunov exponents spectrum	Color
Periodic oscillations	$\Lambda_1 = 0, 0 > \Lambda_2 > \Lambda_3 > \Lambda_4 > \Lambda_5 > \Lambda_6$	red
Two-frequency quasi-periodic oscillations	$\Lambda_1 = \Lambda_2 = 0, 0 > \Lambda_3 > \Lambda_4 > \Lambda_5 > \Lambda_6$	yellow
Three-frequency quasi-periodic oscillations	$\Lambda_1 = \Lambda_2 = \Lambda_3 = 0, 0 > \Lambda_4 > \Lambda_5 > \Lambda_6$	blue
Chaotic oscillations	$\Lambda_1 > 0, \Lambda_2 = 0, 0 > \Lambda_3 > \Lambda_4 > \Lambda_5 > \Lambda_6$	grey
Hyperchaotic oscillations	$\Lambda_1 > \Lambda_2, \Lambda_3 = 0, 0 > \Lambda_4 > \Lambda_5 > \Lambda_6$	black

3.1. Main Dynamical Regimes

First, consider two interacting neurons with model parameters corresponding to a bursting attractor of the square-wave type, which is observed for the set of parameters (2.5) (Fig. 1a). Figure 2 shows the chart of Lyapunov exponents, the color palette is determined in accordance with Table 1. The Neimark – Sacker bifurcation line (l_{NS}) obtained using the XPPAUT numerical bifurcation analysis software package [42] is also marked with a green line in the chart. Figures 2b–2e show characteristic phase portraits and time series.

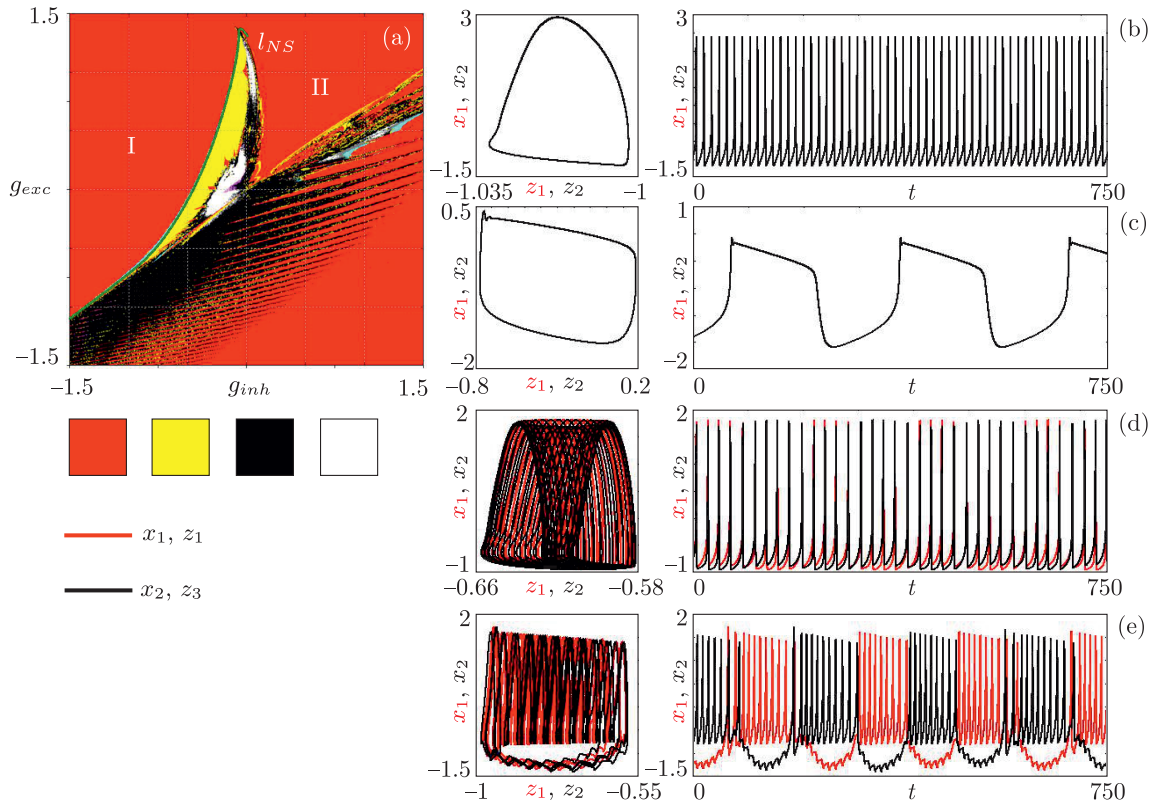

Fig. 2. Chart of Lyapunov exponents and character phase portraits with time series for two coupled Hindmarsh – Rose models (2.2) with (2.5); (b) in-phase complete synchronized spiking, $g_{inh} = -0.75$, $g_{exc} = 0.75$; (c) in-phase complete synchronized degenerated bursting, $g_{inh} = 0.75$, $g_{exc} = 0.75$; (d) quasi-periodic spiking, $g_{inh} = -0.1$, $g_{exc} = 0.75$; (e) $g_{inh} = -0.1$, $g_{exc} = -0.25$. l_{NS} is the line of the Neimark – Sacker bifurcation.

In the chart, it is possible to identify areas of periodic self-oscillations that have a single-turn attractor. This is region **I**, observed for negative values of the strength of the inhibitory coupling; in this case, the excitatory coupling can be either positive or negative. Figure 2b shows an example of an attractor in model (2.2) for $g_{inh} = -0.75$, $g_{exc} = 0.75$. The attractor is a period-1 limit cycle; on the time series, we can distinguish the spike nature of oscillations. Note that the oscillations in the subsystems are in-phase, in Figs. 2b and 2c, we have presented time series of each of the subsystems, while they are completely identical. Thus, in region **I**, we observe complete in-phase synchronization in model (2.2). In region **II**, periodic self-oscillations are also observed. Figure 2c shows an example of a phase portrait and time series. In this case, periodic self-oscillations are also observed, however, the shape of the limit cycle is more complex, and it can be considered as a degenerate plateau bursting attractor. In this case, the observed dynamical regime also responds to complete in-phase synchronization.

In the region of negative values of the inhibitory coupling g_{inh}, one can see the Neimark – Sacker (l_{NS}) bifurcation line. The bifurcation occurs at negative values of the excitatory coupling parameter, g_{exc}, but also continues into the region of positive values of g_{exc}, where it ends. As a result of this bifurcation, the in-phase spike limit cycle loses stability and a stable torus is born, which corresponds to quasi-periodic oscillations. Figure 2d shows an example of a phase portrait, in which one can see a torus for $g_{inh} = -0.1$, $g_{exc} = 0.75$, as well as time series, where one can see that the spike oscillations remained in-phase, but a modulation appeared that has a phase shift for each of the oscillators. Along the Neimark – Sacker bifurcation line, one can distinguish the characteristic tongues of synchronization. An increase in the inhibitory coupling strength g_{inh} leads to the destruction of the torus, and in the chart we see the formation of chaos, as well as hyperchaos, which is observed with positive values of both inhibitory and excitatory couplings. The area of chaos with increasing coupling strength is limited by the tongue of complete synchronization.

Below regions **I** and **II**, periodic regimes corresponding to bursting oscillations, as well as chaotic bursting, are observed. Figure 2e shows an example of a chaotic bursting attractor for $g_{inh} = -0.1$, $g_{exc} = -0.25$. The behavior of the system is antiphase, chaos is characterized by one positive Lyapunov exponent. Next, we will consider in more detail the features of the destruction of the torus and the formation of hyperchaos.

3.2. Formation of Hyperchaos

Let us consider in more detail the area of multidimensional chaos and scenarios for its development. Figure 3a shows an enlarged fragment of the chart of Lyapunov exponents in the area of quasi-periodic regimes and hyperchaos. It is clearly seen that the destruction of a two-frequency torus leads to the formation of chaos and hyperchaos. Two regions of hyperchaos can be distinguished in the parameter plane: a region for positive values of the inhibitory coupling parameter (Fig. 3b), while the excitatory coupling coefficient is also always positive, and a region for negative values of the inhibitory coupling parameter. With a negative inhibitory coupling strength, the excitatory coupling can be either positive or negative. Let us consider in more detail the formation of chaos for the region where the values of the coupling parameters are positive ($g_{exc} \geqslant 0$, $g_{inh} \geqslant 0$), since this is justified from the point of view of the physiological meaning of these parameters.

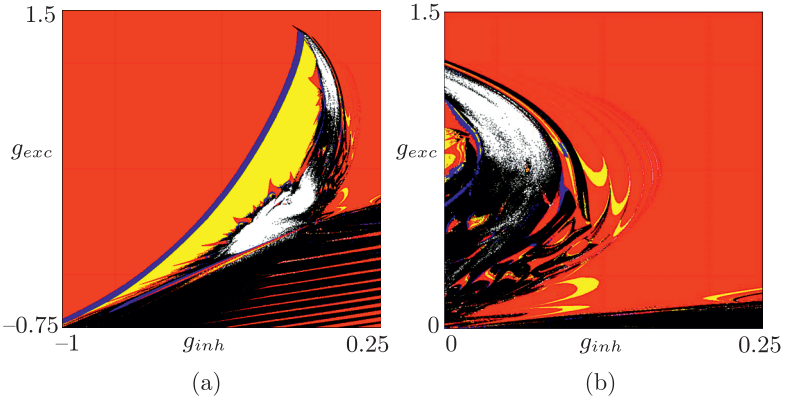

Fig. 3. Enlarged fragments of the chart of Lyapunov exponents in the area of formation of multidimensional chaos for two coupled Hindmarsh – Rose models (2.2) with (2.5).

Let us fix the excitation coupling parameter equal to one ($g_{exc} = 1$) and trace the features of the behavior of the model (2.2). Figure 4 shows the corresponding illustrations: bifurcation trees, bifurcation diagrams, and graphs of Lyapunov exponents.

System (2.2) consists of two identical Hindmarsh – Rose models (2.1). In a coupled system when the oscillators are completely identical it is possible to find a complete in-phase synchronization solution. Such a solution is also called a *synchronous manifold*. The limit cycle $C(5,0)$[1)] represents such kind of solution (see an example of an attractor in Fig. 2b). Figure 4a shows a bifurcation diagram built using XPPAUT (the diagram shows the local maximum amplitude of the dynamical variable x_1, the scale is presented on the right side of panel ($x_1^{\max}$), different colors indicate the dimension of stable and unstable manifolds), which visualizes a synchronous solution for the coupled system. At $g_{inh} \approx -0.1077$, the Neimark – Sacker bifurcation (TR) occurs, as a result of which the limit cycle loses stability and becomes a saddle with a two-dimensional unstable manifold $C(3,2)$. Note that the synchronous manifold, despite the fact that it has lost stability, is preserved in the system. The saddle cycle $C(3,2)$ can be reached from identical initial conditions for subsystems, or

[1)] Using the symbol C(m,n) we denote the limit cycle, the indices in brackets indicate the dimension of the stable (m) and unstable (n) manifolds of the corresponding point in the Poincaré section.

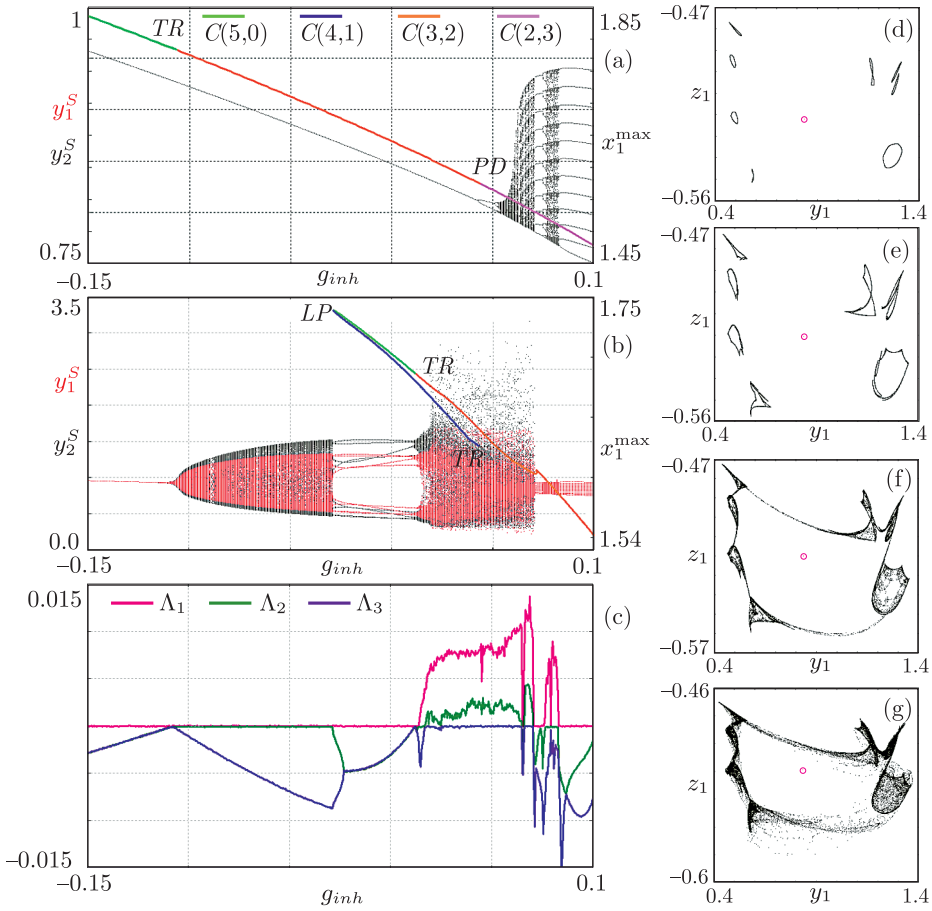

Fig. 4. Formation of chaos in two coupled Hindmarsh – Rose models (2.2) with (2.5), $g_{exc} = 1.0$. (a) bifurcation tree with inherited initial conditions, bifurcation diagram for period-1 limit cycle C; (b) bifurcation tree with fixed initial conditions ($x_{10} = 1.12$, $y_{10} = 2.67$, $z_{10} = -0.42$, $x_{20} = -0.91$, $y_{20} = 3.54$, $z_{20} = -0.38$), bifurcation diagram for period-8 limit cycle; (c) graphs of the three largest Lyapunov exponents for fixed initial conditions. Two-dimensional projections of the Poincaré map formed by the intersection with the plane $x_1 = 0$, (d) $g_{inh} = 0.0127$; (e) $g_{inh} = 0.0145$; (f) $g_{inh} = 0.015$; (g) $g_{inh} = 0.016$. LP is a saddle-node bifurcation line; PD is a period-doubling bifurcation line; TR is a Neimark – Sacker bifurcation line.

by inheriting the initial conditions when constructing a bifurcation tree, as was done for Fig. 4a. In Fig. 4a, together with the bifurcation diagram, a bifurcation tree is also shown in black (the tree was built for the Poincaré section formed by the intersection with the plane $x_1 = 0$, the scale for the tree marked on the left side of panel y_1^S, y_2^S). The saddle cycle corresponding to the synchronous manifold exists with a further increase in the inhibitory coupling parameter; at $g_{inh} \approx 0.04251$, it ungergoes a period-doubling bifurcation (PD), as a result of which the cycle transforms to $C(2,3)$. On the bifurcation tree, one can observe a cascade of period-doubling bifurcations and the formation of a synchronous chaotic attractor. Moreover, this cascade forms a set of cycles with a three-dimensional unstable manifold.

Figure 4b shows projections of bifurcation trees onto two dynamical variables y_1 (red color) and y_2 (black color) depending on inhibitory coupling parameter built without inheritance from nonidentical initial conditions[2)]. This illustration makes it possible to identify nonsynchronous dynamical regimes that arise in model (2.2). The bifurcation tree clearly shows that, as a result of the Neimark – Sacker bifurcation of the synchronous cycle, a torus-attractor is born, which is confirmed by two zero largest Lyapunov exponents in the graphs (Fig. 4c). The torus for each

[2)]In our numerical experiments, we used the fixed initial conditions: $x_{10} = 1.12$, $y_{10} = 2.67$, $z_{10} = -0.42$, $x_{20} = -0.91$, $y_{20} = 3.54$, $z_{20} = -0.38$.

subsystem has a slightly different amplitude, the bifurcation tree clearly shows that the components of each subsystem are different from each other. Also, in Fig. 2d, we observed a phase shift between the time series of each subsystem. With an increase in the parameter of inhibitory coupling, a resonance is observed on the torus, a periodicity window is well traced on the tree, where the limit cycle of period 8 is stable $C1(5,0)$. For this cycle, we constructed a bifurcation diagram using XPPAUT, which is shown in Fig. 4b. This cycle is born as a result of a saddle-node bifurcation, in a pair with a saddle cycle $C2(4,1)$. As the coupling increases further, both cycles undergo a Neimark – Sacker bifurcation, a stable cycle $C1$ at $g_{inh} \approx 0.01212$, and a saddle cycle $C2$ at $g_{inh} \approx 0.04361$. The bifurcation of a stable cycle is accompanied by the birth of a torus, which corresponds to 8 invariant curves in the Poincaré section (8-component torus, see Fig. 4d). As a result of further increase in coupling strength, one can observe resonances on the 8-component torus, then its destruction, the formation of an 8-component chaos (Fig. 4e), and the merging of the components into a single attractor (Fig. 4f). If we look at the graphs of the Lyapunov exponents, we can see that, as a result of these bifurcations, chaos arises (Figs. 4e–4g), and then hyperchaos develops. At $g_{inh} \approx 0.04361$, the hyperchaotic attractor undergoes a crisis and collapses, and in system (2.2), the main oscillatory regime becomes the complete in-phase synchronous regime, which can also be chaotic, but with one positive Lyapunov exponent.

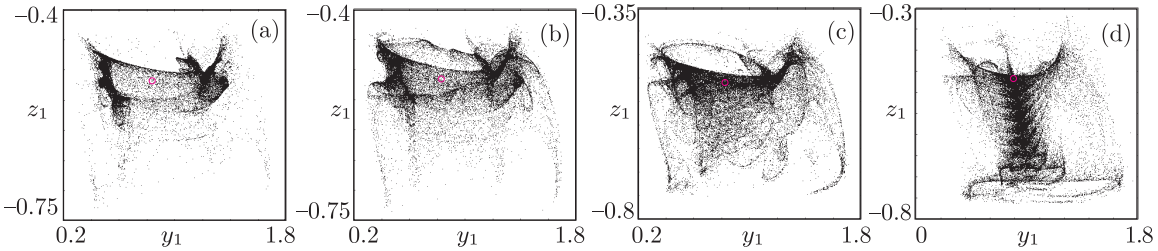

Fig. 5. Formation of hyperchaos in two coupled Hindmarsh – Rose models (2.2) with (2.5), $g_{exc} = 1.0$. Two-dimensional projections of attractors in the Poincaré section formed by the intersection with the plane $x_1 = 0$, (a) $g_{inh} = 0.018$; (b) $g_{inh} = 0.02$; (c) $g_{inh} = 0.03$; (d) $g_{inh} = 0.068$.

The secondary Neimark – Sacker bifurcation creates a set of saddle cycles with a two-dimensional unstable manifold $C2(3,2)$, that can be absorbed by a chaotic attractor, which corresponds to the formation of the Shilnikov attractor [43, 44], while many examples are widely known when the attractor also became hyperchaotic [14, 45–49]. In the system of two coupled Hindmarsh – Rose models (2.2), it is possible to observe such a phenomenon. To illustrate the Shilnikov attractors, Figs. 4d–4g and 5 show a Poincaré map of chaotic attractors. In Figs. 4d–4g, 5, the red circles mark fixed points that correspond to the Poincaré section of a saddle cycle of period 1 with a two-dimensional unstable manifold. The attractors presented in Fig. 4 are well-distanced from the saddle-focus cycle of period 1. It is also clearly seen that the chaotic attractor in Figs. 4e and 4f does not absorb the period-8 limit cycle either, the chaotic attractor has characteristic regions which the phase trajectory does not enter. The chaotic attractor in Fig. 4g has absorbed the period-8 cycle, while it is combined into a single-component attractor, so hyperchaos does not arise.

An increase in the strength of the inhibitory coupling leads to the absorption of the period-1 saddle cycle with a two-dimensional unstable manifold and the development of hyperchaos. Figure 5 shows illustrations of chaotic attractors of this type. In Fig. 5a, a broken invariant curve is traced, while the mapping points visit a small neighborhood of the fixed point of the saddle-focus cycle of period 1. The characteristic areas are also clearly visible, the phase points are concentrated more densely in the regions near fixed points of the period-8 cycle. As the coupling increases, the attractor becomes more complicated and the invariant curve is completely destroyed. It is clearly seen that the fixed points of both the period-8 cycle and period-1 cycle are absorbed by the chaotic attractor.

The Poincaré maps presented above are projections, so we cannot be sure that the saddle cycle is absorbed by the attractor. To check this feature, the minimal distance from the fixed point of the

saddle cycle cross-section to the chaotic attractor was calculated according to the following rule:

$$\rho_{min} = \min(\rho_n),$$
$$\rho_n = \sqrt{\sigma_i(x_i^S - x_{iEP}^S)^2 + (y_i^S - y_{iEP}^S)^2 + (z_i^S - z_{iEP}^S)^2}\ , \tag{3.1}$$

where x_i^S, y_i^S, z_i^S are points of the chaotic attractor in the Poincaré section formed by the intersection with the hyperplane $x_1 = 0$ for each subsystem, $i = 1, 2$; x_{iEP}^S, y_{iEP}^S, z_{iEP}^S are the coordinates of the fixed point of the saddle limit cycle in the Poicaré section, as the period-1 cycle is synchronous we have $x_{1EP}^S = x_{2EP}^S$, $y_{1EP}^S = y_{2EP}^S$, $z_{1EP}^S = z_{2EP}^S$. The obtained data of minimal distances and the values of Lyapunov exponents for the attractors shown in Figs. 4 and 5 are given in Table 2. The data clearly prove that, for a hyperchaotic attractor, the minimal distance from the attractor to the saddle cycle is very small, and we can conclude that the period-1 saddle-focus cycle is absorbed by the chaotic attractor.

Table 2. The minimal distance from an attractor to a fixed point of the period-1 limit cycle in the Poincaré section and Lyapunov exponents for chaotic attractors presented in Figs. 4 and 5

g_{inh}	Λ_1	Λ_2	Λ_3	Λ_4	ρ_{min}
0.0127	0.0	0.0	−0.0004	−0.0219	0.4754
0.0145	0.001	0.0	−0.0041	−0.0157	0.3041
0.015	0.0021	0.0	−0.0037	−0.0152	00431
0.02	0.0063	0.0012	0.0	−0.0166	0.0053
0.03	0.0077	0.0014	0.0	−0.0194	0.0031
0.068	0.0095	0.0001	0.0	−0.0184	0.0007

3.3. Features of Time Series on a Threshold of Hyperchaos Occurence

Let us consider the features of time series and phase portraits of model (2.2) on a threshold and after the formation of a hyperchaotic attractor, paying special attention to the analysis of in-phase and antiphase oscillations of subsystems. To analyze the in-phase oscillations, it is convenient to use the so-called Lissajous figures [50–53]. It is a phase portrait projected onto the plane of the dynamical variable of each subsystem. Figure 6 shows examples of Lissajous figures projected onto the (x_1, x_2) plane. For the case of complete in-phase synchronization of subsystems, the Lissajous figure is a line corresponding to $x_1 = x_2$. If the oscillators are synchronized in antiphase, then the Lissajous figure is a line $x_1 = -x_2$.

Figure 6a corresponds to the case where chaotic behavior is observed in the system of two coupled Hindmarsh – Rose models (2.2). The Lissajous figure is elongated along the main diagonal, but it is symmetrically turned aside from the main diagonal. The phase trajectories do not enter the area of the main diagonal, while there are several points of trajectories intersecting it. On the corresponding time series, we see that each subsystem exhibits spike oscillations, while the amplitude and the period of the spikes change. It can be seen that the spikes themselves are almost synchronous; this corresponds to the cross-section points lying on the main diagonal of the Lissajous figures. Note that the minimum values of the dynamical variables are almost in antiphase. Thus, the phase alternation of each subsystem is observed. As was shown earlier, with an increase in the strength of the inhibitory coupling, the chaotic attractor absorbs a synchronous cycle with a two-dimensional unstable manifold. Figure 6b shows an example of a Lissajous figure immediately after absorption, which corresponds to weak hyperchaos. Figure 6c illustrates a developed hyperchaotic

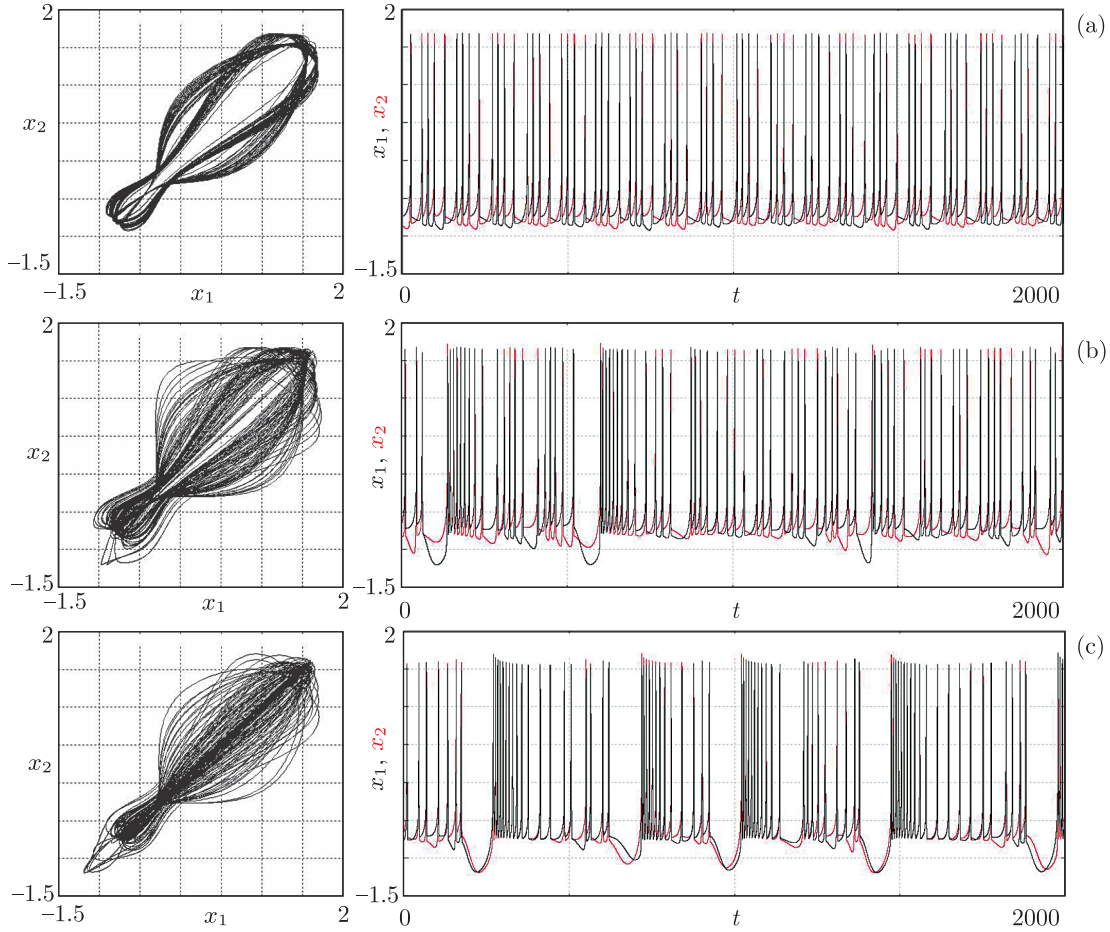

Fig. 6. Formation of in-phase bursting oscillations in two coupled Hindmarsh – Rose models (2.2) with (2.5) associated with hyperchaos occurence, $g_{exc} = 1.0$. Lissajous figures and times series, (a) $g_{inh} = 0.016$; (b) $g_{inh} = 0.03$; (c) $g_{inh} = 0.06$.

attractor, which also contains a saddle-focus cycle corresponding to a synchronous manifold. In the Lissajous figures, we clearly see that trajectories appear that pass through the main diagonal. On the time series in Fig. 6b, there is still an alternation of the phases of the oscillator, as well as cross-sections where the oscillators are in phase. In Fig. 6c, in-phase burstings are formed.

Thus, the appearance of in-phase oscillations in coupled Hindmarsh – Rose oscillators occurs as a result of absorption of the saddle-focus cycle with the two-dimensional unstable manifold corresponding to the synchronous manifold. Moreover, this type of oscillation is hyperchaotic. This feature can be used for diagnostics; in areas of hyperchaos, one can expect the appearance of in-phase synchronization of bursting oscillations.

4. INTERACTION OF NEURON MODELS WITH A PLATEAU BURSTING ATTRACTOR

To study the universality of the phenomena and the scenario described in Section 3, we analyzed the behavior of coupled identical Hindmarsh – Rose systems with a change in the parameter of autonomous subsystems. Figure 7 shows a chart of Lyapunov exponents for two chemically coupled Hindmarsh – Rose models, when autonomous subsystems exhibit a plateau bursting bursting attractor at $a = 2.7$ (see the attractor in Fig. 1b).

The structure of the chart of Lyapunov exponents (Fig. 7) is similar to the case of the interaction of systems with square-wave bursting attractors. In the region of negative values of the inhibitory coupling parameter, a synchronous spike cycle is observed, which undergoes a Neimark – Sacker

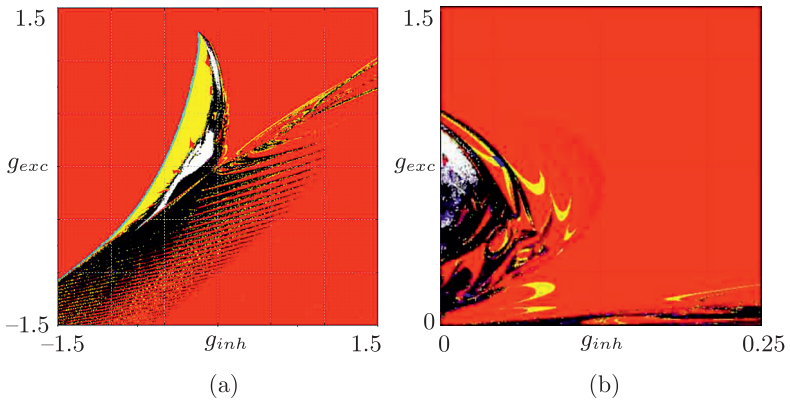

Fig. 7. Chart of Lyapunov exponents and its enlarged fragment in the area of formation of multidimensional chaos for two coupled Hindmarsh – Rose models (2.2) with $a = 2.7$, $b = 9.0$, $c = 5.0$, $\alpha = 1.6$, $\lambda = 10$, $\mu = 0.001$.

bifurcation and the birth of a torus. The destruction of the torus and the formation of Shilnikov attractors leads to the appearance of hyperchaotic behavior. Also, two areas of hyperchaos are localized on the parameter plane. The enlarged fragment (Fig. 7b) shows the region of positive values of the coupling parameters. As can be seen in this case, the areas with hyperchaos have decreased, but are still present. For positive values of the coupling parameter g_{inh}, there are no regions of quasi-periodic regime, so the destruction of the torus occurs already at negative values of the coupling parameter.

5. CONCLUSIONS

A study of two identical models of neurons interacting through a chemical coupling is carried out. As an example of the neuron model the Hindmarsh – Rose systems is used. It is shown that taking into account two types of couplings can lead to the excitation of chaotic and hyperchaotic oscillations in the ensemble. The structure of parameter planes depending on the coupling parameters is described, on which the regions of chaos and hyperchaos are localized. The scenario of hyperchaos formation is described. The basic dynamical regime is the synchronous spike limit cycle, which undergoes a Neimark – Sacker bifurcation. As a result of this bifurcation, a stable torus is born, which does not have the property of in-phase synchronization. The destruction of the torus occurs via resonances and cascades of Neimark – Sacker bifurcations. Further development of chaos leads to a homoclinic bifurcation, as a result of which an in-phase saddle-focus cycle with a two-dimensional unstable manifold is absorbed by a chaotic attractor, which leads to the appearance of hyperchaos. It is shown that the formation of hyperchaos leads to the appearance of in-phase synchronization of bursting oscillations.

The picture of dynamical regimes described above is universal and is observed for another choice of subsystems parameters, as well as a change of the type of the bursting attractor.

ACKNOWLEDGMENTS

The authors thank Dr. Alexey Kazakov and Prof. Igor Belykh for useful discussions of this problem.

FUNDING

This work is supported by the Russian Science Foundation (project no. 20-71-10048, Sections 2.2, 3, 5). NVS, AAB are partially supported by the Laboratory of Dynamical Systems and Applications NRU HSE, grant of the Ministry of Science and Higher Education of the RF, ag. no. 075-15-2022-1101 (Sections 2.1, 4).

CONFLICT OF INTEREST

The authors declare that they have no conflicts of interest.

REFERENCES

1. Kuramoto, Y., *Chemical Oscillations, Waves and Turbulence*, Berlin: Springer, 1984.
2. Litvak, A. G. and Tokman, M. D., Electromagnetically Induced Transparency in Ensembles of Classical Oscillators, *Phys. Rev. Lett.,* 2002, vol. 88, no. 9, 095003, 4 pp.
3. Moskalenko, O. I., Koronovskii, A. A., Hramov, A. E., and Boccaletti, S., Generalized Synchronization in Mutually Coupled Oscillators and Complex Networks, *Phys. Rev. E,* 2012, vol. 86, no. 3, 036216, 9 pp.
4. Zakharova, A., *Chimera Patterns in Networks: Interplay between Dynamics, Structure, Noise, and Delay,* Cham: Springer, 2020.
5. Pikovsky, A., Rosenblum, M., and Kurths, J., *Synchronization: A Universal Concept in Nonlinear Sciences,* Cambridge Nonlinear Sci. Ser., vol. 12, New York: Cambridge Univ. Press, 2001.
6. Mosekilde, E., Maistrenko, Yu., and Postnov, D., *Chaotic Synchronization: Applications to Living Systems,* World Sci. Ser. Nonlinear Sci. Ser. A Monogr. Treatises, vol. 42, River Edge, N.J.: World Sci. Publ., 2002.
7. González-Miranda, J. M., *Synchronization and Control of Chaos: An Introduction for Scientists and Engineers,* London: Imperial College Press, 2004.
8. Rössler, O. E., An Equation for Hyperchaos, *Phys. Lett. A,* 1979, vol. 71, no. 2, pp. 155–157.
9. Cannas, B. and Cincotti, S., Hyperchaotic Behaviour of Two Bi-Directionally Coupled Chua Circuits, *Int. J. Circuit Theory Appl.,* 2002, vol. 30, no. 6, pp. 625–637.
10. Rasmussen, J., Mosekilde, E., and Reick, C., Bifurcations in Two Coupled Rössler Systems, *Math. Comput. Simul.,* 1996, vol. 40, nos. 3–4, pp. 247–270.
11. Postnov, D., Vadivasova, T., Sosnovtseva, O., Balanov, A., Anishchenko, V., and Mosekilde, E., Role of Multistability in the Transition to Chaotic Phase Synchronization, *Chaos,* 1999, vol. 9, no. 1, pp. 227–232.
12. Yanchuk, S. and Kapitaniak, T., Chaos–Hyperchaos Transition in Coupled Rössler Systems, *Phys. Lett. A,* 2001, vol. 290, nos. 3–4, pp. 139–144.
13. Čenys, A., Tamaševičius, A., Baziliauskas, A., Krivickas, R., and Lindberg, E., Hyperchaos in Coupled Colpitts Oscillators, *Chaos Solitons Fractals,* 2003, vol. 17, nos. 2–3, pp. 349–353.
14. Stankevich, N. V., Dvorak, A., Astakhov, V., Jaros, P., Kapitaniak, M., Perlikowski, P., and Kapitaniak, T., Chaos and Hyperchaos in Coupled Antiphase Driven Toda Oscillators, *Regul. Chaotic Dyn.,* 2018, vol. 23, no. 1, pp. 120–126.
15. Perlikowski, P., Yanchuk, S., Wolfrum, M., Stefanski, A., Mosiolek, P., and Kapitaniak, T., Routes to Complex Dynamics in a Ring of Unidirectionally Coupled Systems, *Chaos,* 2010, vol. 20, no. 1, 013111, 10 pp.
16. Stankevich, N. and Volkov, E., Chaos–Hyperchaos Transition in Three Identical Quorum-Sensing Mean-Field Coupled Ring Oscillators, *Chaos,* 2021, vol. 31, no. 10, 103112, 12 pp.
17. Stankevich, N. V., Kuznetsov, A. P., and Seleznev, E. P., Chaos and Hyperchaos Arising from the Destruction of Multifrequency Tori, *Chaos Solitons Fractals,* 2021, vol. 147, Paper No. 110998, 8 pp.
18. Rinzel, J., A Formal Classification of Bursting Mechanisms in Excitable Systems, in *Mathematical Topics in Population Biology, Morphogenesis and Neurosciences,* E. Teramoto, M. Yumaguti (Eds.), Lecture Notes in Biomath., vol. 71, Berlin: Springer, 1987.
19. Izhikevich, E. M., Neural Excitability, Spiking and Bursting, *Internat. J. Bifur. Chaos Appl. Sci. Engrg.,* 2000, vol. 10, no. 6, pp. 1171–1266.
20. Shilnikov, A. and Cymbalyuk, G., Transition between Tonic Spiking and Bursting in a Neuron Model via the Blue-Sky Catastrophe, *Phys. Rev. Lett.,* 2005, vol. 94, no. 4, 048101, 4 pp.
21. Shilnikov, A., Calabrese, R. L., and Cymbalyuk, G., Mechanism of Bistability: Tonic Spiking and Bursting in a Neuron Model, *Phys. Rev. E (3),* 2005, vol. 71, no. 5, 056214, 9 pp.
22. Izhikevich, E. M., *Dynamical Systems in Neuroscience: The Geometry of Excitability and Bursting,* Cambridge, Mass.: MIT Press, 2007.
23. Pankratova, E. V. and Kalyakulina, A. I., Environmentally Induced Amplitude Death and Firing Provocation in Large-Scale Networks of Neuronal Systems, *Regul. Chaotic Dyn.,* 2016, vol. 21, nos. 7–8, pp. 840–848.
24. Koronovskii, A. A., Hramov, A. E., Grubov, V. V., Moskalenko, O. I., Sitnikova, E. Yu., and Pavlov, A. N., Coexistence of Intermittencies in the Neuronal Network of the Epileptic Brain, *Phys. Rev. E,* 2016, vol. 93, no. 3, 032220, 5 pp.

25. Nikitin, D., Omelchenko, I., Zakharova, A., Avetyan, M., Fradkov, A. L., and Schöll, E., Complex Partial Synchronization Patterns in Networks of Delay-Coupled Neurons, *Philos. Trans. Roy. Soc. A,* 2019, vol. 377, no. 2153, 20180128, 19 pp.
26. Ruzzene, G. Omelchenko, I., Sawicki, J., Zakharova, A., Schöll, E., and Andrzejak, R. G., Remote Pacemaker Control of Chimera States in Multilayer Networks of Neurons, *Phys. Rev. E,* 2020, vol. 102, no. 5, 052216, 9 pp.
27. Pankratova, E. V., Kalyakulina, A. I., Stasenko, S. V., Gordleeva, S. Yu., Lazarevich, I. A., and Kazantsev, V. B., Neuronal Synchronization Enhanced by Neuron-Astrocyte Interaction, *Nonlinear Dyn.,* 2019, vol. 97, no. 1, pp. 647–662.
28. Belykh, I. and Shilnikov, A., When Weak Inhibition Synchronizes Strongly Desynchronizing Networks of Bursting Neurons, *Phys. Rev. Lett.,* 2008, vol. 101, no. 7, 078102, 4 pp.
29. Jalil, S., Belykh, I., and Shilnikov, A., Fast Reciprocal Inhibition Can Synchronize Bursting Neurons, *Phys. Rev. E (3),* 2010, vol. 81, no. 4, 045201, 4 pp.
30. Reimbayev, R. and Belykh, I., When Transitions between Bursting Modes Induce Neural Synchrony, *Internat. J. Bifur. Chaos Appl. Sci. Engrg.,* 2014, vol. 24, no. 8, 1440013, 9 pp.
31. Belykh, I., Reimbayev, R., and Zhao, K., Synergistic Effect of Repulsive Inhibition in Synchronization of Excitatory Networks, *Phys. Rev. E (3),* 2015, vol. 91, no. 6, 062919, 10 pp.
32. Reimbayev, R., Daley, K., and Belykh, I., When Two Wrongs Make a Right: Synchronized Neuronal Bursting from Combined Electrical and Inhibitory Coupling, *Philos. Trans. Roy. Soc. A,* 2017, vol. 375, no. 2096, 20160282, 19 pp.
33. Chay, T. R., Effects of Extracellular Calcium on Electrical Bursting and Intracellular and Luminal Calcium Oscillations in Insulin Secreting Pancreatic Beta-Cells, *Biophys. J.,* 1997, vol. 73, no. 3, pp. 1673–1688.
34. Zeldenrust, F., Wadman, W. J., and Englitz, B., Neural Coding with Bursts-Current State and Future Perspectives, *Front. Comput. Neurosci.,* 2018, vol. 12, Art. 48, 14 pp.
35. Gibson, J. R., Beierlein, M., and Connors, B. W., Two Networks of Electrically Coupled Inhibitory Neurons in Neocortex, *Nature,* 1999, vol. 402, no. 6757, pp. 75–79.
36. Hindmarsh, J. L. and Rose, R. M., A Model of Neuronal Bursting Using Three Coupled First Order Differential Equations, *Proc. R. Soc. Lond. Ser. B Biol. Sci.,* 1984, vol. 221, no. 1222, pp. 87–102.
37. Shilnikov, A. and Kolomiets, M., Methods of the Qualitative Theory for the Hindmarsh – Rose Model: A Case Study. A Tutorial, *Internat. J. Bifur. Chaos Appl. Sci. Engrg.,* 2008, vol. 18, no. 8, pp. 2141–2168.
38. Barrio, R., Angeles Martínez, M., Serrano, S., and Shilnikov, A., Macro- and Micro-Chaotic Structures in the Hindmarsh – Rose Model of Bursting Neurons, *Chaos,* 2014, vol. 24, no. 2, 023128, 11 pp.
39. Garashchuk, I. R., Asynchronous Chaos and Bifurcations in a Model of Two Coupled Identical Hindmarsh – Rose Neurons, *Russian J. Nonlinear Dyn.,* 2021, vol. 17, no. 3, pp. 307–320.
40. Garashchuk, I. R. and Sinelshchikov, D. I., Excitation of a Group of Two Hindmarsh – Rose Neurons with a Neuron-Generated Signal, *Russian J. Nonlinear Dyn.,* 2023, vol. 19, no. 1, pp. 19–34.
41. Benettin, G., Galgani, L., Giorgilli, A., and Strelcyn, J.-M., Lyapunov Characteristic Exponents for Smooth Dynamical Systems and for Hamiltonian Systems: A Method for Computing All of Them: P. 1: Theory, *Meccanica,* 1980, vol. 15, no. 1, pp. 9–20.
42. Ermentrout, G. B., *Simulating, Analyzing, and Animating Dynamical Systems: A Guide to XPPAUT for Researchers and Students,* Software, Environments, and Tools, vol. 14, Philadelphia, Pa.: SIAM, 2002.
43. Gonchenko, A. S., Gonchenko, S. V., and Shilnikov, L. P., Towards Scenarios of Chaos Appearance in Three-Dimensional Maps, *Nelin. Dinam.,* 2012, vol. 8, no. 1, pp. 3–28 (Russian).
44. Gonchenko, A. S., Gonchenko, S. V., Kazakov, A. O., and Turaev, D. V., Simple Scenarios of Onset of Chaos in Three-Dimensional Maps, *Internat. J. Bifur. Chaos Appl. Sci. Engrg.,* 2014, vol. 24, no. 8, 1440005, 25 pp.
45. Garashchuk, I. R., Sinelshchikov, D. I., Kazakov, A. O., and Kudryashov, N. A., Hyperchaos and Multistability in the Model of Two Interacting Microbubble Contrast Agents, *Chaos,* 2019, vol. 29, no. 6, 063131, 16 pp.
46. Stankevich, N., Kuznetsov, A., Popova, E., and Seleznev, E., Chaos and Hyperchaos via Secondary Neimark – Sacker Bifurcation in a Model of Radiophysical Generator, *Nonlinear Dyn.,* 2019, vol. 97, no. 4, pp. 2355–2370.
47. Stankevich, N., Kazakov, A., and Gonchenko, S., Scenarios of Hyperchaos Occurrence in 4D Rössler System, *Chaos,* 2020, vol. 30, no. 12, 123129, 16 pp.
48. Sataev, I. R. and Stankevich, N. V., Cascade of Torus Birth Bifurcations and Inverse Cascade of Shilnikov Attractors Merging at the Threshold of Hyperchaos, *Chaos,* 2021, vol. 31, no. 2, Paper No. 023140, 8 pp.
49. Shykhmamedov, A., Karatetskaia, E., Kazakov, A., and Stankevich, N., Scenarios for the Creation of Hypercaotic Attractors in 3D Maps, *Nonlinearity,* 2023, vol. 36, no. 7, pp. 3501–3541.

50. French, A. P., The Superposition of Periodic Motions, in *Vibrations and Waves,* Boca Raton, Fla.: CRC, 1971, pp. 19–39.
51. Rulkov, N. F. and Lewis, C. T., Subharmonic Destruction of Generalized Chaos Synchronization, *Phys. Rev. E,* 2001, vol. 63, no. 6, 065204, 4 pp.
52. Palmer, K., Ridgway, T., Al-Rawi, O., Johnson, I., and Poullis, M., Lissajous Figures: An Engineering Tool for Root Cause Analysis of Individual Cases: A Preliminary Concept, *J. Extra Corpor. Technol.,* 2011, vol. 43, no. 3, pp. 153–156.
53. Stankovski, T., Analogue Simulation and Synchronization Analysis of Non-Autonomous Oscillators, in *Tackling the Inverse Problem for Non-Autonomous Systems: Application to the Life Sciences,* Cham: Springer, 2014, pp. 109–117.